J|A|C|S
ARTICLES

Published on Web 07/16/2010

Crystal Structure of Chiral γPNA with Complementary DNA Strand: Insights into the Stability and Specificity of Recognition and Conformational Preorganization

Joanne I. Yeh,*,† Boris Shivachev,† Srinivas Rapireddy,‡ Matthew J. Crawford,‡ Roberto R. Gil,‡ Shoucheng Du,† Marcela Madrid,§ and Danith H. Ly*,‡

Department of Structural Biology, University of Pittsburgh Medical School 1036 BST3, 3501 Fifth Avenue, Pittsburgh, Pennsylvania 15260, Department of Chemistry and Center for Nucleic Acids Science and Technology (CNAST), Mellon Institute, Carnegie Mellon University, 4400 Fifth Avenue, Pittsburgh, Pennsylvania 15213, and Pittsburgh Supercomputing Center, Pittsburgh, Pennsylvania 15213

Received August 26, 2009; E-mail: jiyeh@pitt.edu; dly@andrew.cmu.edu

Abstract: We have determined the structure of a PNA−DNA duplex to 1.7 Å resolution by multiple-wavelength anomalous diffraction phasing method on a zinc derivative. This structure represents the first high-resolution 3D view of a hybrid duplex containing a contiguous chiral PNA strand with complete γ-backbone modification ("γPNA"). Unlike the achiral counterpart, which adopts a random-fold, this particular γPNA is already preorganized into a right-handed helix as a single strand. The new structure illustrates the unique characteristics of this modified PNA, possessing conformational flexibility while maintaining sufficient structural integrity to ultimately adopt the preferred P-helical conformation upon hybridization with DNA. The unusual structural adaptability found in the γPNA strand is crucial for enabling the accommodation of backbone modifications while constraining conformational states. In conjunction with NMR analysis characterizing the structures and substructures of the individual building blocks, these results provide unprecedented insights into how this new class of chiral γPNA is preorganized and stabilized, before and after hybridization with a cDNA strand. Such knowledge is crucial for the future design and development of PNA for applications in biology, biotechnology, and medicine.

Introduction

Synthetic chemistry has played a crucial role in advancing the field of biology, biotechnology, and medicine in the past several decades, with particular impact in the area of nucleic acid recognition. With the human genome[1,2] and the genomes of many biomedically relevant organisms completely sequenced,[3] along with the unprecedented scale of biological and biomedical research being conducted where many novel genes, and gene products and regulatory elements are being discovered at an incredibly rapid pace,[4−8] there is an urgent need to develop molecules that can recognize and bind to these nucleic acid targets in a sequence-specific manner. Such molecules could be developed into a wide range of applications, from molecular tools for probing and manipulating nucleic acid structures and functions, and regulation of gene expression, to therapeutic and diagnostic reagents for the treatment and detection of genetic diseases. Natural oligonucleotides comprised of a sugar phosphodiester backbone, such as DNA and RNA, could be employed for this purpose; however, they are not ideally suited for many of these in vivo applications due to their susceptibility to degradation by nucleases. To overcome this deficiency, much of the effort to date has been focused on the design and development of nucleic acid mimics that can withstand such enzymatic degradation in the cellular milieu. As a result, a large collection of such a class of oligonucleotides have been developed,[9−12] but like their natural counterparts they are not cell permeable. Poor cellular uptake along with other issues, including nonspecific binding and cytoxicity, have been the source of frustration and unreliability in many antisense and antigene applications.[13] From that standpoint, it is important to be able to modify the structures and chemical functionalities of these reagents further, with ease and flexibility, so that their

† University of Pittsburgh Medical School.
‡ Carnegie Mellon University.
§ Pittsburgh Supercomputing Center.

(1) Lander, E. S.; et al. *Nature* **2001**, *409*, 860–921.
(2) Venter, C.; et al. *Science* **2001**, *291*, 1304–1351.
(3) Croucher, N. J. *Nat. Rev. Microbiol.* **2009**, *7*, 621.
(4) Lockhart, D. J.; Winzeler, E. A. *Nature* **2000**, *405*, 827–836.
(5) Lagos-Quintana, M.; Rauhut, R.; Lendeckel, W.; Tuschl, T. *Science* **2001**, *294*, 853–858.
(6) Lewis, B. P.; Burge, C. B.; Bartel, D. P. *Cell* **2005**, *120*, 15–20.
(7) Hesselberth, J. R.; Chen, X.; Zhang, Z.; Sabo, P. J.; Sandstrom, R.; Reynolds, A. P.; Thurman, R. E.; Neph, S.; Kuehn, M. S.; Noble, W. S.; Fields, S.; Stamatoyannopoulos, J. A. *Nat. Methods* **2009**, *6*, 283–289.
(8) Gargiulo, G.; Levy, S.; Bucci, G.; Romanenghi, M.; Fornasari, L.; Beeson, K. Y.; Goldberg, S. M.; Cesaroni, M.; Ballarini, M.; Santoro, F.; Bezman, N.; Frige, G.; Gregory, P. D.; Holmes, M. C.; Strausberg, R. L.; Pelicci, P. G.; Urnov, F. D.; Minucci, S. *Dev. Cell* **2009**, *16*, 466–481.
(9) De Mesmaeker, A.; Haner, R.; Martin, P.; Moser, H. E. *Acc. Chem. Res.* **1995**, *28*, 366–374.
(10) Wengel, J. *Acc. Chem. Res.* **1999**, *32*, 301–310.
(11) Nielsen, P. E. *Acc. Chem. Res.* **1999**, *32*, 624–630.
(12) Summerton, J. E. *Lett. Pept. Sci.* **2004**, *10*, 215–236.
(13) Stein, C. A. *Nat. Biotechnol.* **1999**, *17*, 209.

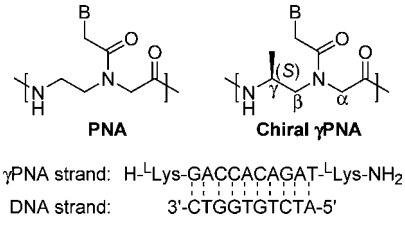

Figure 1. Chemical structures of PNA and chiral γPNA unit along with the nucleobase sequence of the crystallized γPNA−DNA hybrid duplex.

physical attributes could be selectively tuned to meet the applications in-hands.

One such promising class of nucleic acid mimics developed in the last two decades is the peptide nucleic acid (PNA).[14] PNA differs from most nucleic acid mimics in that it contains an entirely redesigned backbone skeleton, consisting of *N*-(2-aminoethyl)glycine instead of the usual sugar phosphodiester backbone (Figure 1). The charge-neutral backbone allows PNA to hybridize to cDNA or RNA strand with high affinity,[15] while the unnatural polyamide linkage enables PNA to evade recognition and degradation by proteases and nucleases.[16] These properties make PNA an attractive reagent for numerous applications in biology and medicine.[17] Among its other appealing attributes include the ease and flexibility of synthesis because of the acyclic and achiral backbone. The structure of PNA can be easily modified, unlike many other classes of nucleic acid mimics developed to date, which are highly constrained and already embedded with numerous stereogenic centers.[9,10,12] So far, a large number of structural modifications have been made to the backbone of PNA.[18−23] Among these, changes at the γ-position show the most promise because of the simplicity and flexibility of synthesis, and the benefits that they confer on the hybridization properties of PNA.[24−33]

Recently, we showed that PNA, which, as an individual strand does not have a well-defined conformation, can be preorganized into either a right-handed or a left-handed helix by installing a stereogenic center at the γ-backbone position.[31] That derived from D-amino acids adopts a left-handed helix, while that derived from L-amino acids adopts a right-handed helix; however, only the right-handed helical PNA is able to hybridize to DNA or RNA with high affinity and sequence selectivity.[31] To the best of our knowledge, γPNA is the only class of oligonucleotide currently developed capabilities of invading mixed-sequence double helical B-form DNA (B-DNA) without requiring "tail-clamp" anchoring[34,35] or simultaneous binding to both strands of the DNA double helix,[36] with the recognition occurring via canonical Watson−Crick (WC) base-pairing.[37,38] The fact that any chemical group can be installed at this position, and that the synthesis can be accomplished in a few simple steps from commercially available and relatively inexpensive L-amino acids, provides an even greater impetus for exploring the structure−function relationship of PNA at the γ-backbone position. Understanding the molecular principles that govern the structural organization and binding properties of γPNA is an important first step toward developing a more effective nucleic acid platform for targeting DNA and RNA. Towards this effort, we describe the crystal structure of a γPNA−DNA duplex, solved and refined to 1.7 Å resolution along with NMR analysis of the individual building blocks. The results yield insights into structural determinants that direct the helical folding of γPNA and improve the thermodynamic stability of the bound complex.

Results

We present the crystal structure of a uniquely preorganized γPNA−DNA duplex, containing a chiral PNA strand with complete γ-backbone modification, which, as an individual strand, is already preorganized into a right-handed helical structure (Figures 1 and S1, Supporting Information).[31] The duplex structure was solved through a three-wavelength zinc anomalous phasing approach with the parameters shown in Table 1; *ab initio* phasing was required as initial molecular replacement (MR) trials using various duplex PNA, B-DNA, and PNA−DNA search models did not yield promising solutions. Comparison of the refined hybrid γPNA−DNA with PNA−DNA duplex structures shows rmsd differences of over 3 Å, with the lowest rmsd values of 1.5 Å, explaining the lack of convergence during MR attempts. These structural differences and new structural features are further elaborated below. Overall, the crystal packing of neighboring γPNA−DNA duplexes is organized orthogonally and propagated along the *b* and *c* crystallographic axis leading to two networks of packing interactions that create unusually large cavities, resulting in a solvent content of ~63% (Figure S2a−c). These packing interactions may reflect the rigidity of the helices that originates from γ-backbone modification on the PNA strand.

Overall Structure. The γPNA−DNA duplex forms a right-handed helix with a helical twist of 23.6 Å, a rise of 3.1 Å, and

(14) Nielsen, P. E.; Egholm, M.; Berg, R. H.; Buchardt, O. *Science* **1991**, *254*, 1497–1500.
(15) Jensen, K. K.; Orum, H.; Nielsen, P. E.; Norden, B. *Biochemistry* **1997**, *36*, 5072–5077.
(16) Demidov, V. V.; Potaman, V. N.; Frank-Kamenetskii, M. D.; Egholm, M.; Buchard, O.; Sonnichsen, S. H.; Nielsen, P. E. *Biochem. Pharmacol.* **1994**, *48*, 1310–1313.
(17) Nielsen, P. E. *Mol. Biotechnol.* **2004**, *26*, 233–248.
(18) Uhlmann, E.; Peyman, A.; Breipohl, G.; Will, D. W. *Angew. Chem., Int. Ed.* **1998**, *37*, 2796–2823.
(19) Beck, F.; Nielsen, P. E. *Artificial DNA: Methods and Applications*; CRC Press: Boca Raton, FL, 2003; Vol. 2003, pp 91−114.
(20) Kumar, V. A.; Ganesh, K. N. *Acc. Chem. Res.* **2005**, *38*, 404–412.
(21) Pokorski, J. K.; Witschi, M. A.; Purnell, B. L.; Appella, D. H. *J. Am. Chem. Soc.* **2004**, *126*, 15067–15073.
(22) Pensato, S.; Saviano, M.; Romanelli, A. *Expert Opin. Biol. Ther.* **2007**, *7*, 1219–1232.
(23) Corradini, R.; Sforza, S.; Tedeschi, T.; Marchelli, R. *Chirality* **2007**, *19*, 269–294.
(24) Kosynkina, L.; Wang, W.; Liang, T. C. *Tetrahedron Lett.* **1994**, *35*, 5173–5176.
(25) Falkiewicz, B.; Kolodziejczyk, A. S.; Liberek, B.; Wisniewski, K. *Tetrahedron* **2001**, *57*, 7909–7917.
(26) Wu, Y.; Xu, J. C. *Tetrahedron* **2001**, *57*, 8107–8113.
(27) Tedeschi, T.; Sforza, S.; Corradini, R.; Marchelli, R. *Tetrahedron Lett.* **2005**, *46*, 8395–8399.
(28) Englund, E. A.; Appella, D. H. *Org. Lett.* **2005**, *7*, 3465–3467.
(29) Dose, C.; Seitz, O. *Org. Lett.* **2005**, *7*, 4365–4368.
(30) De Koning, M. C.; Petersen, L.; Weterings, J. J.; Overhand, M.; Van der Marel, G. A.; Filippov, D. V. *Tetrahedron* **2006**, *62*, 3248–3258.
(31) Dragulescu-Andrasi, A.; Rapireddy, S.; Frezza, B. M.; Gayathri, C.; Gil, R. R.; Ly, D. H. *J. Am. Chem. Soc.* **2006**, *128*, 10258–10267.
(32) Englund, E. A.; Appella, D. H. *Angew. Chem., Int. Ed.* **2007**, *46*, 1414–1418.
(33) Sforza, S.; Tedeschi, T.; Corradini, R.; Marchelli, R. *Eur. J. Org. Chem.* **2007**, 5879–5885.
(34) Bentin, T.; Larsen, H. J.; Nielsen, P. E. *Biochemistry* **2003**, *42*, 13987–13995.
(35) Kaihatsu, K.; Shah, R. H.; Zhao, X.; Corey, D. R. *Biochemistry* **2003**, *42*, 13996–14003.
(36) Lohse, J.; Dahl, O.; Nielsen, P. E. *Proc. Natl. Acad. Sci. U.S.A.* **1999**, *96*, 11804–11808.
(37) He, G.; Rapireddy, S.; Bahal, R.; Sahu, B.; Ly, D. H. *J. Am. Chem. Soc.* **2009**, *131*, 12088–12090.
(38) Chenna, V.; Rapireddy, S.; Sahu, B.; Ausin, C.; Pedroso, E.; Ly, D. H. *ChemBioChem* **2008**, *9*, 2388–2391.

Table 1. Data Collection Phasing and Refinement Statistics for MAD γPNA−DNA Duplex Structure[a]

crystal data			
space group		$P2_12_12_1$	
cell dimensions			
a, *b*, *c*, Å		48.19, 52.57, 61.15	
α, *β*, *γ*, deg		90, 90, 90	
independent molecules		2	
diffraction data			
	peak	inflection	remote
wavelength, Å	1.28449	1.28513	1.27196
resolution, Å	1.85	1.87	1.91
reflections	11 443	10 883	10 720
completeness, %	90.7(54.1)	91.1(55.3)	97.4(85.9)
$I/\sigma(I)$	20.4(2.8)	22.1(3.2)	24.2(4.0)
redundancy	5.3(3.0)	5.3(3.2)	5.7(4.4)
R_{merge}, %	7.4(33.5)	7.3(34.2)	6.5(31.0)
refinement			
reflections used		11 992	
resolution, Å		10−1.7	
R_{work}/R_{free}, %		21.2/23.5	
no. of atoms		1082	
PNA−DNA		815	
ligand/ion		10	
water		257	
B-factors, Å^2			
overall		35.5	
γPNA strands		34.1	
DNA strands		36.9	
structural water		36.6	
Zn/Mg		37.5	
water		34.5	
rmsd			
bond lengths, Å		0.015	
bond angles, deg		1.5	

[a] Values in parentheses are for the highest-resolution shell.

a pitch of 15 base-pairs per turn. These values were based on the average of two structures (Table 2). Two duplexes were found within the asymmetric unit, related by a noncrystallographic (NCS) 2-fold axis of rotation, with the duplexes differing mainly at the terminal residues, which could be attributed to end-fraying (Figure S2d). Structural differences between the two duplexes in the asymmetric unit are more pronounced in the γPNA than in the DNA strand, corresponding to a translational shift of ∼1.5 Å away from the helical axis of the γPNA strand and encompassing the terminal three bases. In the γPNA−DNA duplex, the carbonyl oxygens of the peptide backbone project outward toward the solvent, while those in the bridge that connect the backbone to the nucleobase point toward the C-terminus (Figure 2a and b). The (*S*)-Me groups at the γ-positions also point toward the solvent, confirming the result obtained from molecular modeling by Appella and co-workers,[32] but are in a trans configuration to the carbonyl oxygens in the backbone. Overall, the structure adopts a P-form helix, with greater resemblance to A-form than B-form DNA (Tables S2−4). Of the four lysine residues in the two duplexes in the asymmetric unit, which were added to improve water solubility, two could be resolved in the electron density maps, both of which reside at the C-terminus. Flexibility of the long lysine side-chains and lack of intra- or interstrand interactions to limit their conformational states may explain why the other two lysines cannot be resolved in the electron density maps. Particularly interesting is the finding of periodic and well-defined water bridges that connect the base to the backbone in the γPNA strand, possibly providing a structural explanation to the enhanced stabilization found in this preorganized duplex structure, as described below.

Interstrand Interactions. Classical Watson−Crick (W−C) base-pairing interactions are found in the γPNA−DNA duplex, which form a right-handed helix. Representative electron densities and hydrogen-bonding interactions are shown in Figure 2c. The base-pair stacking pattern closely resembles that of an A-form DNA, with the base-pairs stacked nearly perpendicular to the helical and crystallographic axes (mean base-tilt 0.3° and 2.3°). A continuous base-pair stacking is observed throughout the helix, continuing from the termini to the next asymmetric unit. The DNA residue *d*C10 is stacked with the symmetry related DNA strand residue *d*A1 (*d* refers to DNA strand, 5′-end corresponds to position 1), and γPNA residue G*p*1 (*p* refers to γPNA strand, N-terminus corresponds to position 1) is stacked with the symmetry related γPNA strand residue T*p*10. The packing interactions lead to formation of large cavities ∼20 Å in diameter along the helical axis with a base-pair *x*-displacement of −5.5/−6.2 Å (Table 1S), resulting in a wide and deep major groove and a narrow and shallow minor groove. The helical parameters for the γPNA strands are similar to those previously reported for the αPNA−DNA duplex (Tables 2 and S5).[39]

Hydration, Cation Interactions, and Structural Stabilization. The asymmetric unit contains 257 water molecules, many of which are first hydration-shell waters, ordered and well-defined, and may be responsible for providing additional stabilization to the γPNA−DNA duplex. We have classified the water molecules according to their interactions with the γPNA and DNA strands in the duplex. The "PNA water bridges" connect the backbone amide to the adjacent N-terminal nucleobase in the γPNA strand. Although bridging waters have been found in other nucleic acid structures,[39,42,44,46] they are unique in this case because they are found at every base of the γPNA strand (Figure 3), likely leading to enhanced conformational stabilization augmented through formation of hydrogen-bonding interactions. These water bridges directly connect the backbone amide NH to N3 of the purine or O2 of the pyrimidine nucleobase. The second "DNA water bridges" are involved in interactions with the DNA backbone, bridging the oxygen atoms in the phosphate backbone to the adjacent nitrogen atom of the nucleobase (data not shown). In addition to water bridges, we found zinc atoms coordinating the ribose phosphate groups and

(39) Menchise, V.; De Simone, G.; Tedeschi, T.; Corradini, R.; Sforza, S.; Marchelli, R.; Capasso, D.; Saviano, M.; Pedone, C. *Proc. Natl. Acad. Sci. U.S.A.* **2003**, *100*, 12021–12026.
(40) Eriksson, M.; Nielsen, P. E. *Nat. Struct. Biol.* **1996**, *3*, 410–413.
(41) Betts, L.; Josey, J. A.; Veal, J. M.; Jordan, S. R. *Science* **1995**, *270*, 1838–1841.
(42) Eldrup, A. B.; Nielsen, B. B.; Haaima, G.; Rasmussen, H.; Kastrup, J. S.; Christensen, C.; Nielsen, P. E. *Eur. J. Org. Chem.* **2001**, 1781–1790.
(43) Petersson, B.; Nielsen, B. B.; Rasmussen, H.; Larsen, I. K.; Gajhede, M.; Nielsen, P. E.; Kastrup, J. S. *J. Am. Chem. Soc.* **2005**, *127*, 1424–1430.
(44) Rasmussen, H.; Kastrup, J. S.; Nielsen, J. N.; Nielsen, J. M.; Nielsen, P. E. *Nat. Struct. Biol.* **1997**, *4*, 98–101.
(45) Rasmussen, H.; Liljefors, T.; Petersson, B.; Nielsen, P. E.; Kastrup, J. S. *J. Biomol. Struct. Dyn.* **2004**, *21*, 495–502.
(46) Haaima, G.; Rasmussen, H.; Schmidt, G.; Jensen, D. K.; Kastrup, J. S.; Stafshede, P. W.; Norden, B.; Buchardt, O.; Nielsen, P. E. *New J. Chem.* **1999**, *23*, 833–840.
(47) Bloomfield, V. A.; Crothers, D. M.; Tinoco, I. J.; Hearst, J. E.; Wemmer, D. E.; Killman, P. A.; Turner, D. H. *Nucleic Acids: Structures, Properties, and Functions*; University Science Books: Mill Valley, CA, 2000; pp 88−91.
(48) Lavery, R.; Sklenar, H. *J. Biomol. Struct. Dyn.* **1988**, *6*, 63–91.
(49) Lavery, R.; Sklenar, H. *Curves 5.1, Computer Program*; Institut de Biologie Physico-Chimique, CNRS; Paris, 1996.

Table 2. Comparison of Helical Parameters (Averaged)[a]

entry	structure	type	twist [deg]	rise [Å]	base tilt [deg]	displacement [Å]	bases per turn
1	this work, (AC)	γPNA−DNA	23.9	3.2	0.3	−5.5	15.1
	this work, (BD)	γPNA−DNA	23.3	2.9	2.3	−6.3	15.5
2	1NR8[39]	αPNA−DNA	23.2	3.5	0.2	−3.8	15.5
3	1PDT[40]	PNA−DNA	28.0	3.3		3.8	13
4	1PNN-triplex[41]	PNA_2−DNA	22.9	3.4	5.1	6.8	16
5	1HZS-(bT)-R[42]	PNA−PNA	18	3.7	0.1	3.3	18
	1HZS-(bT)-L		−18	3.8	0.7	2.7	18
6	1XJ9-R[43]	PNA−PNA	19.1	3.4	0.0	−3.5	19
	1XJ9-L		−18.0	3.3	0.0	7.9	20
7	1PUP-R[44]	PNA−PNA	19.8	3.2	1.0	8.3	18
8	1RRU-R[45]	PNA−PNA	20.5	3.2	0.0	7.7	18
	1RRU-L	PNA−PNA	19	3.4	0.0	6.6	18
9	1QPY-(N-Me)-R1[46]	PNA−PNA	18.9	3.8	0.2	4.8	18
	1QPY-(N-Me)-R2	PNA−PNA	19	3.8	0.1	4.9	18
	1QPY-(N-Me)-L1	PNA−PNA	−20	3.5	0.0	7.2	18
	1QPY-(N-Me)-L2	PNA−PNA	−20	3.5	0.3	7.2	18
10	A-DNA[47]		32.7	2.6	−4.5	−4.5	11
11	B-DNA[47]		36.0	3.4	−0.1	0.0	10

	sugar pucker	intrastrand P distance [Å]	dislocation of BP from helix axis [Å]	rise [Å]	tilt [deg]
A-DNA	C3′-*endo*	5.9	4.0−4.9 major groove	2.56−3.29	10−20 positive
B-DNA	C2′-*endo*	7.0	−0.02−1.8 minor groove	3.03−3.37	−5.9−16.4 negative

[a] AC and BD refer to the two duplexes in the asymmetric crystallographic unit, with one duplex being the pairing of strands A and C, and the other of being strands B and D. *P* = interstrand phosphate−phosphate distance, BP = base-pair. Helical parameters were analyzed with CURVES.[48,49]

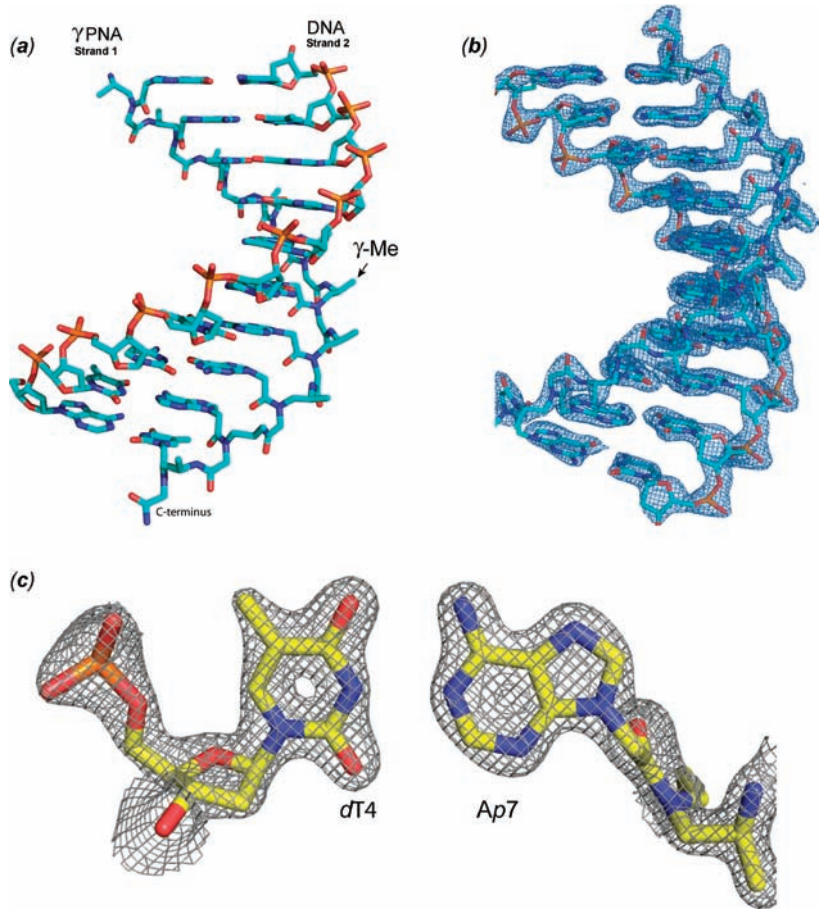

Figure 2. (a) Structure of the γPNA−DNA double helix. (b) Experimental electron density map of the double helix. (c) Representative unweighted $2F_o - F_c$ electron density map contoured at 1.8σ showing the base-pairing between *d*T4 in the DNA and A*p*7 in the γPNA strand.

the γPNA nucleobases, located near N7 of the *d*G bases of the DNA moiety (Figure S3). The extensive interactions observed in the structure and inability to grow diffracting γPNA−DNA crystals in the absence of zinc metals suggest that these ions play a crucial role in enhancing lattice interactions, a feature that could potentially be exploited in structural determinations of other γPNA complexes. The locations of the zinc ions are central to the two duplexes in the asymmetric unit, assembling

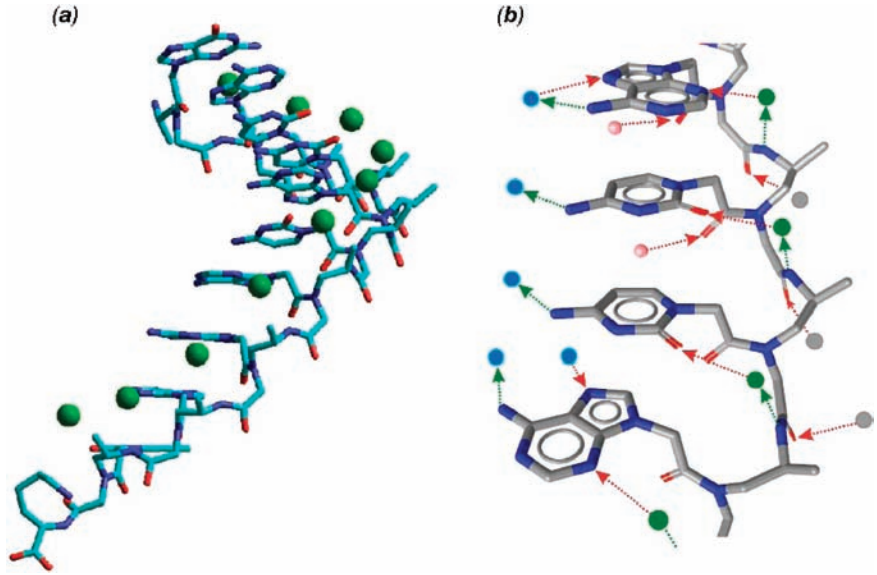

Figure 3. (a) A view of the γPNA strand (the DNA strand is omitted for clarity). The "water bridges" are present between all of the backbone amide NH and nucleobases (purine-N3 or pyrimidine-O2) enhancing the stability of the γPNA helix. (b) γPNA interactions with surrounding solvent molecules (γPNA strand, residues 6−9). Watson−Crick hydrogen-bonding interactions between γPNA and DNA strands are not included for clarity. The structural waters bridging the "backbone−water−nucleobase" are represented in green, the waters interacting with backbone carbonyl oxygens are shown in gray, and the ones involved in HB interactions with the nucleotides are shown in blue with waters connected to the methylene-carbonyl in red.

these molecules into an intertwined dimer approximating an "X" shape. We ruled out the possibility of Zn^{2+} perturbing the structure of the duplex by performing CD and UV-melting experiments with and without Zn^{2+}. Our result showed that the CD profiles of the two samples are virtually identical to one another (Figure S4a), indicating that Zn^{2+} does not interfere with the structure of γPNA−DNA double helix. The melting transitions (T_m's) of the duplex are ∼10 °C lower with divalent cations Mg^{2+} and Zn^{2+} as compared to that with monovalent Na^+ (Figure S4b). A similar finding has been reported for PNA−DNA.[50] The difference in the T_m's can be explained in terms of counterion release upon hybridization of PNA (or γPNA in this case) to DNA in contrast to counterion association observed with formation of DNA duplex.

Helical Preorganization. Stabilization through introduction of chiral center at the γ-backbone position of PNA has been reported,[27,28,31,51] with introduction of each chiral unit resulting in an increase in the T_m of the PNA−DNA duplex by ∼3 °C and PNA−RNA by ∼2 °C. The basis for this highly enhanced thermal stabilization can now be further understood from analysis of the collective structural results. We had previously determined the solution structure of the single-strand CT γPNA dimer by NMR.[31] Comparison of γPNA strands from the current γPNA−DNA duplex to single-strand CT γPNA dimer reveals that the γPNA strands are structurally similar to one another in three aspects: backbone arrangement, carboxymethylene bridge projection, and nucleobase orientation (Figure 4). In both the duplex and the single-strand forms, the (*S*)-Me group at the γ-position is in a trans configuration with the bridge, which, in turn, is in trans with the backbone carbonyl oxygen within the same unit. The striking similarities between the two structures, in both the bound and the unbound states, suggest that the molecular interactions that direct the folding of the hybrid duplex also direct the folding of the individual γPNA strands.

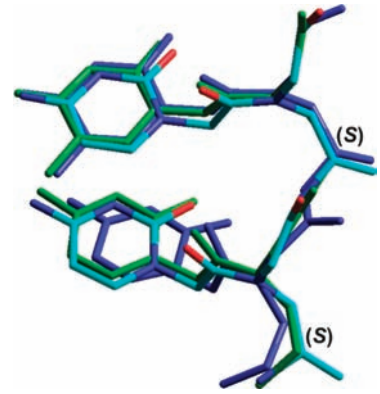

Figure 4. Superposition of PNA strands from the current γPNA−DNA (cyan) and published PNA−DNA duplex determined by X-ray crystallography (green),[39] and single-strand CT γPNA dimer determined by NMR (blue).[31]

Structural Organization of Individual Building Blocks. To determine the origin of helical induction, whether conformational preorganization of γPNA occurs as the result of oligomerization due to base-stacking or is intrinsic to the individual building blocks, we determined the solution structures of a series of γPNA monomers. A total of four monomers, containing glycine (unmodified), L-alanine, L-valine, and L-isoleucine amino acid side-chain at the γ-backbone position, were examined. These amino acid side-chains, which are incremental in size, were specifically designed to test the effect of steric crowding at the γ-position on the conformation of monomers. Structural assignments were made on the basis of the following NMR experiments: 1D ^{1}H NMR, phase-sensitive double quantum filtered COSY (DQFCOSYPH), rotating frame Overhauser spectroscopy (ROESY), and ^{1}H,^{13}C-heteronuclear single-quantum correlation spectroscopy (HSQC), with the results shown in Figure S5 and Table S6. These experiments were necessary to better resolve the resonances of the proton signals in the 3−5 ppm regions of the spectra due to the complexity of the system caused by formation of rotamers. Our data revealed

(50) Tomac, S.; Sarkar, M.; Ratilainen, T.; Wittung, P.; Nielsen, P. E.; Norden, B.; Graeslund, A. *J. Am. Chem. Soc.* **1996**, *118*, 5544–5552.
(51) Rapireddy, S.; He, G.; Roy, S.; Armitage, B. A.; Ly, D. H. *J. Am. Chem. Soc.* **2007**, *129*, 15596–15600.

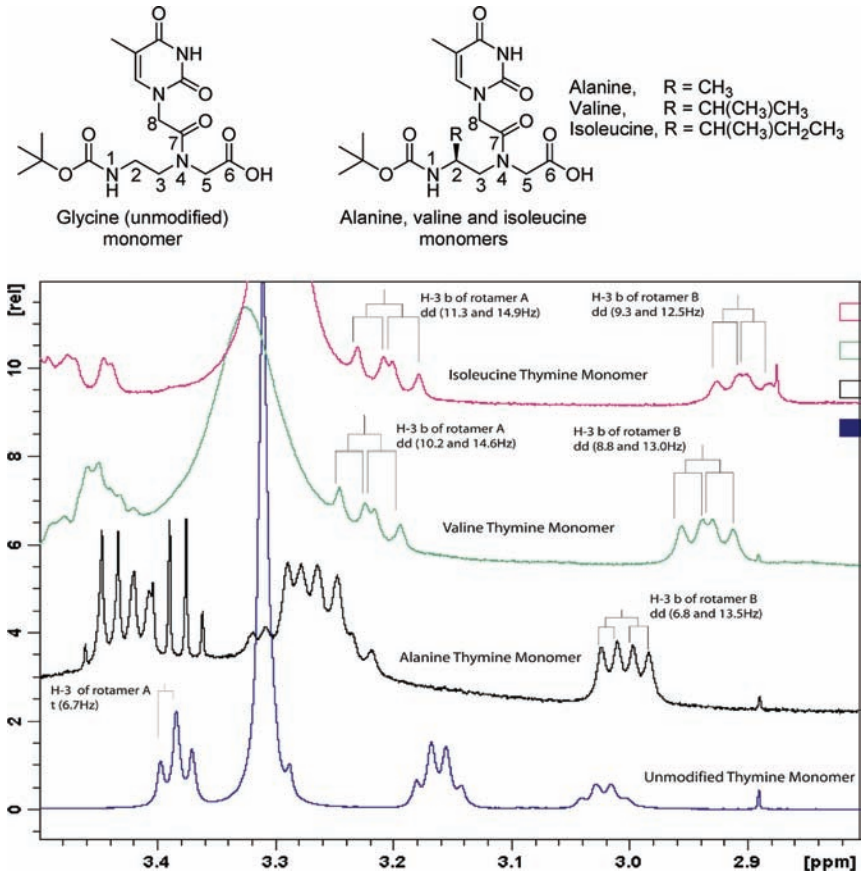

Figure 5. ^{1}H NMR spectrum showing the region of a preferred conformation. The unmodified (glycine) and alanine monomers do not show structure given that the ^{3}J-coupling constants are ~6−7 Hz. The valine and isoleucine monomers show a preferred conformation given that the ^{3}J-coupling constants are ~13−15 and 10 Hz for the A part and ~12 and 3 Hz for the B part of the AB system.

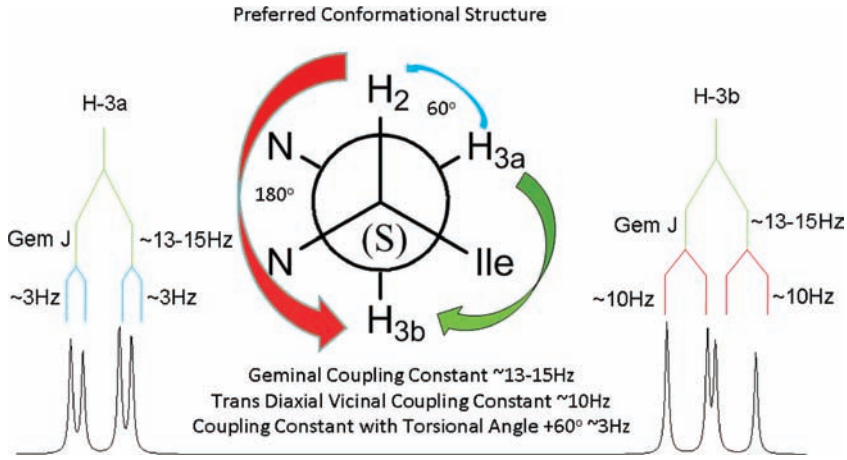

Figure 6. Newman projection showing the preferred conformation around the C2−C3 bond for the C-2*S* configuration in the isoleucine backbone. NMR splitting patterns showing estimated *J*-coupling constants according to the Karplus relationship, consistent with the structure adopting a right-handed helix.

that glycine and alanine monomers do not have a preferred conformation, apparent from the average ^{3}J-coupling constants of ~6−7 Hz involving protons H-2, H-3a, and H-3b (Figure 5, Table S6). Such degeneracy in the coupling constants would only occur if there is free rotation around the C2−C3 bond. On the other hand, valine and isoleucine monomers showed nonaverage coupling constants, with values consistent with the Karplus relationship of ^{3}J-coupling as a function of the dihedral angle between H-2, H-3a, and H-3b (Figure 6).[5,6] The signals corresponding to protons H-3a and H-3b appeared as the AB part of an ABX system, where X corresponds to proton H-2. The A component (H-3a) appeared as a doublet of doublets of ~13−15 and ~3 Hz, and the B component (H-3b) appeared as a doublet of doublets of ~13−15 and ~10 Hz. The ~10 Hz coupling constant corresponds to a trans diaxial relationship (180°) between H-3b and H-2, and the ~3 Hz coupling constant corresponds to an equatorial to axial relationship (+60°) between H-3a and H-2, in agreement with the Karplus relationship. The ~13−15 Hz coupling constant corresponds to the germinal coupling (^{2}J) between H-3a and H-3b. In this case, the rotation

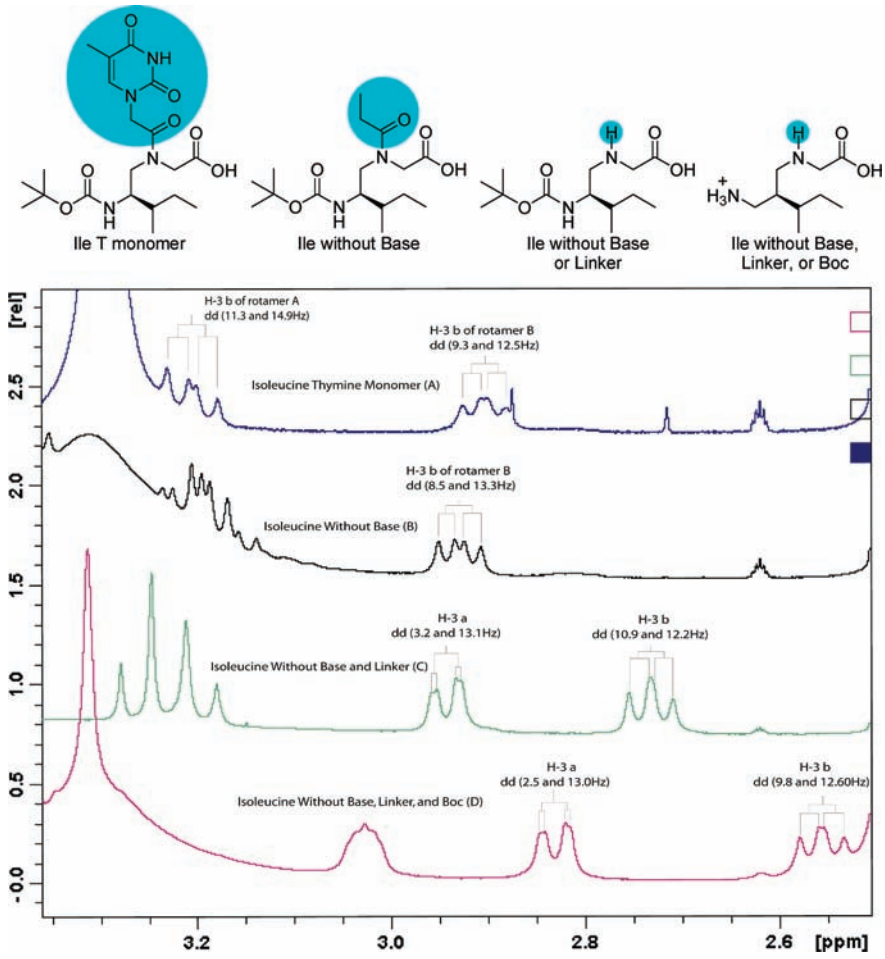

Figure 7. ^{1}H NMR spectrum showing the region of a preferred conformation. All of the isoleucine substructures showed a preferred conformation in the 2.5−3.4 ppm regions. Similar to the isoleucine monomer, the ^{3}J-coupling constants are ∼13−15 and 10 Hz for the A component and ∼12 and 3 Hz for the B component of the AB system, indicating the presence of the structurally organized systems.

around C2−C3 bond is restricted, presumably due to the large isopropyl and *sec*-butyl side-chain of valine and isoleucine, respectively. The fact that the alanine monomers do not have a preferred conformation as individual units but that they do when covalently linked together into an oligomer suggests that base-stacking between adjacent units plays an important role in determining the helical sense as well as in stabilizing the conformation of the helix. The extent of base-stacking between individual units is not known, but it must be sufficiently large to stabilize a CT dimer, as observed in our earlier work.[31]

Origin of Structural Organization in γPNA Monomers. To further pinpoint the source of structural organization in monomers, we prepared several substructures of the isoleucine building block in which the thymine nucleobase, carboxymethylene linker, and Boc protecting group were systematically removed and determined their solution structures using the same set of NMR experiments mentioned in the previous section. The complete structural assignments are shown in Figure S6 and Table S7. To our surprise, we found that in all of the precursors, even the one without the nucleobase, linker and Boc protecting group still retained structural features. This is reflected in the nonaverage splitting patterns of the H-2, and H-3a and H-3b proton system (Figure 7). To rule out the possibility of structural organization occurring as the result of solvent effect, with the sample prepared in DMSO-d_6, we also performed the experiments in D_2O. The ^{1}H NMR proton signals for the isoleucine substructure without the nucleobase and carboxymethylene linker in D_2O are similar to those observed in DMSO-d_6 (Figure S7), indicating that structural organization is independent of solvent in this case. These results show that installation of a bulky, *sec*-butyl side-chain at the γ-backbone position can lock the isoleucine substructure in a specific conformation. Structural preference in this case does not depend on the nucleobase, carboxymethylene linker, or Boc protecting group, because their removal had no affect on the ability of corresponding substructure to adopt a preferred conformation.

Discussion

In recent years, our understanding of PNA interactions with DNA, RNA, and PNA has improved considerably as the result of atomic resolution structural studies via X-ray and NMR. However, to date, only a limited number of such structures have been solved; these include the structures of two PNA−DNA,[39,40] one PNA−RNA,[52] one PNA_2−DNA,[41] and five PNA−PNA complexes.[42,44,46,53,54] Of the two PNA−DNA duplexes, only one contained PNA backbone modifications, and it was made at the α- rather than at the γ-position.[39] Correlating the influence of specific chemical modifications made in the backbone of PNA

(52) Brown, S. C.; Thomson, S. A.; Veal, J. M.; Davis, D. G. *Science* **1994**, *265*, 777–780.
(53) He, W.; Hatcher, E.; Balaeff, A.; Beratan, D. N.; Gil, R. R.; Madrid, M.; Achim, C. *J. Am. Chem. Soc.* **2008**, *130*, 13264–13273.
(54) He, W.; Crawford, M. J.; Rapireddy, S.; Madrid, M.; Gil, R. R.; Ly, D. H.; Achim, C. *Mol. Biol. Syst.* **2010**, DOI: 10.1039/c002254c.

to conformational organization and recognition properties provides insights for rational design of PNA. The PNA under study contains a new chiral backbone, which distinguishes it from the previously characterized PNAs. The modified PNA backbone, (*S*)-*N*-(2-aminopropyl)glycine, has an additional methyl group at the γ-position (Figure 1). These chiral γPNAs are relatively facile to prepare, and, once synthesized, they are preorganized into a right-handed helix, with the characteristic profile similar to that of a corresponding γPNA−DNA hybrid duplex (Figure S1). These helical γPNAs exhibit high binding affinity and sequence selectivity for DNA, RNA, and γPNA, and are able to invade mixed-sequence double helical B-DNA at physiological temperature,[37,38,51] a feat that cannot be accomplished with classical PNA containing natural nucleobases. Obtaining a three-dimensional structure of such a γPNA−DNA duplex is valuable because it yields information not only about the molecular interactions that stabilize the double helix but also insights into how such interactions may direct the helical folding of the individual γPNA strands. It should be pointed out that γPNAs are not the only acylic, chiral PNA oligomers that adopt helical motifs as individual strands. Sforza and co-workers[55] showed that PNAs containing α-backbone modifications also adopt a helical motif, but generally the stability of the helix is weaker for αPNAs than for γPNAs, as inferred from the amplitude of the CD signals, which closely correlates with the extent of base-stacking. Likewise, single-stranded DNA and RNA molecules have also been shown to adopt a preferred helical conformation,[56−60] but they are structurally more rigid and contain more chiral centers than γPNA.

Usually, hybridization of PNA to DNA, RNA, or PNA results in the formation of a duplex structure with helical parameters that differ from those of the canonical A- and B-forms, named the P-form.[41] The P-form helical motif has a significant *x*-displacement, a small twist angle, and a wide and deep major groove. The helical parameters for the current structure fall within this category, with *x*-displacement of −5.5/−6.3 Å, a small twist angle of 23.9/23.3°, and a wide and deep major groove. The γPNA−DNA duplex, accommodating 15 base-pairs per turn, is underwound as compared to B-DNA, which has 10 base-pairs per turn. Thus, the P-form is the preferred conformation of PNA in the duplex (Table 2). The conformations of the PNA strand, with and without γ-backbone modification, differ considerably from one another in backbone torsion angles (Table S5).[40] These changes reflect the addition of the methyl group at the γ-position. Despite these differences, however, the overall topological features align with those of the P-form, indicating that this motif can accommodate a range of geometrical modifications. This aspect may be considered from two completely opposite points of view: first as a proof of the high flexibility of the PNA backbone skeleton, which can accommodate such structural modification, and, second, as a proof of the "constrained flexibility" of PNA's overall conformation because the P-helical form is conserved. The latter is supported by the fact that γPNA−DNA adopts a structure that is intermediate between the A- and B-form DNA, similar to the structure of E-DNA[61,62] and DNA with a peculiar G_3C_3 track,[63] indicating that DNA accommodates the PNA exigencies. This is why the observed DNA backbone variations are more pronounced. The changes in the DNA backbone torsion angles, relative to the two other PNA−DNA crystal structures,[39,40] yield values closer to the A-type DNA (Table S2). Additionally, the γ (O5′−C5′−C4′−C3′) torsion angle values are somewhat different, a fact that is related to the observed variation in the sugar ring puckering. In one of the strands, most of the sugar rings adopt the C3′-*endo* conformation (Table S3). In the second DNA strand, the sugar puckering is more evenly distributed (Table S4). These structural results reveal that PNA strand functions as the template in driving the ultimate topological conformation of the γPNA−DNA hybrid duplex. The specific molecular interactions found and characterized in this structure are fundamental to the future design of PNA for biological and biomedical applications.

A significant number of solvent water molecules are involved in structural stabilization. In both γPNA strands, a water molecule bridges the amide NH to the nucleobase N or O atom. In this structure, all such available positions are occupied by water molecules or Mg^{2+} ions from the crystallization conditions (Figure 3a). In contrast to other reported PNA structures, full occupancy of these sites via water bridges is not consistently achieved. This can be explained by the relative stability of the backbone as all of the carbonyl oxygens of the carboxymethyl moieties point toward the C-terminal direction of the γPNA backbone, while the backbone carbonyl groups project outward toward the solvent. The behavior of the carboxymethyl moiety is similar in all of the reported PNAs, but the classical backbone conformation seems to possess more flexibility as the backbone NH and carbonyl oxygens may swap positions.[39,42,44,46] In the latter case, the bridging hydrogen-bonding interactions between backbone C═O···water···nucleobase (N or O) appears to be entropically less favorable, and the bridging water site may remain unoccupied. Consequently, the role of the water molecules structurally incorporated in the γPNA strand seems important for its stabilization. One could envision the use of these water sites for optimizing γPNA stability, through enhancement of the tricentered "backbone···water···nucleobase" bonding interactions. This could be achieved by replacing the water molecules with ions or through the design of a new backbone with altered acceptor/donor groups. Inversely, the PNA flexibility may also be affected by preventing the tricentered interactions, as described above. The rigidity induced by the γ-methyl group leads to an overall structural propensity that is propagated through the particular intermolecular lattice packing interactions seen in the crystal.

While the N3/O2 atoms of the nucleobases are involved in key "backbone···water···nucleobase" stabilization bridges, the remaining donors and acceptors from the nucleobase and backbone of γPNA strands form hydrogen bonds with the surrounding solvent molecules (Figure 3b). Depending on the number of available sites, one or two water molecules are involved in this γPNA−solvent interaction. If packing interac-

(55) Sforza, S.; Haaima, G.; Marchelli, R.; Nielsen, P. E. *Eur. J. Org. Chem.* **1999**, 197–204.
(56) Holcomb, D. N.; Tinoco, I. J. *Biopolymers* **1965**, *3*, 121–133.
(57) Leng, M.; Felsenfeld, G. *J. Mol. Biol.* **1966**, *15*, 455–466.
(58) Poland, D.; Vournakis, J. N.; Harold, A. *Biopolymers* **1966**, *4*, 223–235.
(59) Brahms, J.; Michelson, A. M.; Van Holde, K. E. *J. Mol. Biol.* **1966**, *15*, 467–488.
(60) Vesnaver, G.; Breslauer, K. J. *Proc. Natl. Acad. Sci. U.S.A.* **1991**, *88*, 3569–3573.
(61) Vargason, J. M.; Eichman, B. F.; Ho, P. S. *Nat. Struct. Biol.* **2000**, *7*, 758–761.
(62) Vargason, J. M.; Henderson, K.; Ho, P. S. *Proc. Natl. Acad. Sci. U.S.A.* **2001**, *98*, 7265–7270.
(63) Ng, H.-L.; Kopka, M. L.; Dickerson, R. E. *Proc. Natl. Acad. Sci. U.S.A.* **2000**, *97*, 2035–2039.

tions prevent the inclusion of a higher number of water molecules, the only available water acts simultaneously as donor and acceptor (the two cases are illustrated through water···adenine interaction in Figure 3b). All backbone carbonyl groups of γPNA strands are also hydrogen bonded to solvent water molecules or Mg^{2+} ions, and thus the backbone flexibility is additionally restricted. Even the oxygens from the carboxymethylene bridges participate in the structure stabilization. The γPNA strands, although generally considered as hydrophobic, are strongly involved in hydrogen-bonding interactions with the surrounding water molecules.

Even though individual contribution resulting from the nonbridging γPNA−solvent interactions may not be as significant for overall structural stabilization as those incorporated within the γPNA strands, the additive effects may be quite substantial. Modifying solvation effects introduces another means of enhancing PNA solubility, by targeting sufficient backbone modifications while balancing the preservation of crucial WC nucleobase interactions. Beyond the first and second hydration shells, the remaining bulk waters are distributed with a higher fraction located near the backbone of the DNA strands. These water molecules bridge to the backbone phosphates. Even though these water molecules indirectly interact with the duplex, they contribute to structural fidelity by forming an extensive solvation network. Intriguingly, despite the importance of water associations in stabilizing DNA, the distinct and periodic water interactions found around the γPNA strand are less pronounced around the DNA strand, further highlighting the unique role that waters may play in conformational stabilization of γPNA.

γPNAs in the single-strand (determined by NMR) and in the hybrid duplex form (determined by X-ray crystallography) adopt a strikingly similar conformation (Figure 4). Superposition of their structures reveals that, in both cases, the carboxymethylene bridge that connects the backbone to the nucleobase is in a trans configuration with the methyl group at the γ-position of the same unit, which, in turn, is in trans with the backbone carbonyl oxygen of the adjacent N-terminal unit. The main differences between the two structures are the arrangement of the backbone carbonyl oxygens and the nucleobases. In the single-strand form, the carbonyl oxygens are projected further away from the helix, while the nucleobases slide closer underneath one another. This could be the result of base-stacking, which would give single-strand γPNA a more efficient $\pi-\pi$ interaction. A slight shift of the nucleobases toward the backbone may cause the backbone carbonyl oxygens to slide away from the helix to minimize the steric and/or electrostatic repulsion with the carbonyl oxygens in the bridge. We suggested in our previous study that the helical sense of γPNA is determined by the configuration of the chemical group at the γ-position.[31] In this case, the *S*-configuration prefers a right-handed helix because the methyl group at this position favors a trans diaxial relationship with N4′ to minimize steric clash. A left-handed helix would force the two groups to be in a gauche configuration, which is highly unfavorable. The energy difference between the two states is estimated to be in the range of 3−4 kcal/mol, corresponding to greater than 99% of the population existing in one helical sense.[31] Energy minimizations of the backbone subunits using the molecular mechanics force field MMX in HyperChem revealed molecular arrangements similar to those found in the X-ray and NMR structures (Figure 8). These results confirm our previous modeling study, which suggested that helical induction occurs as the result of steric clash between the methyl group at the γ-position and N4′, which determines the helical sense of the oligomer (Figure 8b−d). This interpretation, however, is in reference to the oligomer. As individual units, alanine monomers do not have a preferred conformation, apparent from the degeneracy in the ^3J-coupling constants involving protons H-2, H-3a, and H-3b (Figure 5, Table S6). The fact that they adopt a helical motif when conjugated into an oligomer indicates that base-stacking between adjacent units plays an important role in determining the helical sense of γPNA as well as in stabilizing the helical motif. Monomers containing valine and isoleucine side-chain, on the other hand, have defined conformations as individual units, presumably due to the large isopropyl and *sec*-butyl group at the γ-position that prevent the backbone from freely rotating around the C2−C3 bond. The steric clash that prevents this rotation must be between the substituent at the C-2′ (γ-position) and N4′, because removal of the nucleobase, carboxymethelene linker, or Boc protecting group had no effect on structural organization. To rule out the possibility of structural organization occurring as the result of solvent effect, specific to DMSO, we also performed the experiment in D_2O. In both cases, nondegeneracy in the coupling constants of protons H-2, H-3a, and H-3b was observed (Figure S7), indicating that structural organization is an intrinsic property of this particular class of molecules and not the result of solvent effect. Our analyses of the structures of the individual building blocks by solution NMR and the oligomers by X-ray crystallography suggest an additional layer for fine-tuning the rigidity of the γPNA backbone, and thus the hybridization properties, by varying the degree of steric crowding of the chemical group at the γ-backbone position, as demonstrated with the isopropyl and *sec*-butyl side-chains.

Overall, our results indicate that the helical sense of γPNA, whether it adopts a right-handed or left-handed helix, is determined by the steric clash between the substituent at C-2′ and N4′. Once seeded, the helical induction propagates from the C- to N-terminus in a cooperative fashion constrained by a series of steric clashes in the backbone and between the backbone and the nucleobase, followed by base-stacking that stabilizes the helix. The unidirectionality of the helical induction has been experimentally determined in our recent study.[31] The γ-C2′ prefers a trans diaxial relationship with the backbone carbonyl oxygen of the adjacent N-terminal unit, which, in turn, prefers a similar trans diaxial conformation with the methylene bridge within the same unit (Figure 8b−d). The reverse, N- to C-terminal, helical induction does not occur because of the free rotation around the C2−C3 bond in the N-terminal γPNA unit. The rotation around this bond is restricted when the γPNA unit is placed at the adjacent C-terminal position. Once formed, the helix remains relatively stable even at temperature as high as 80 °C, inferred from temperature-dependent CD measurements (Figure S1a, inset).

Helical motifs are ubiquitous in nature. They are found in the secondary structures of peptides and nucleic acids, such as α-helical peptides and double helical DNA, and in the tertiary and quarternary structures of proteins, such as collagens, microtubules, and coating proteins of certain viruses, as well in a large variety of non-natural systems.[64,65] While a great deal has been learned about these systems, it remains a challenge to design new classes of biopolymers that would fold into a specific helical motif and contain the appropriate chemical functionalities needed to carry out a specific biological function. Although

(64) Gellman, S. H. *Acc. Chem. Res.* **1998**, *31*, 173–180.
(65) Hill, D. J.; Mio, M. J.; Prince, R. B.; Hughes, T. S.; Moore, J. S. *Chem. Rev.* **2001**, *101*, 3893–4011.

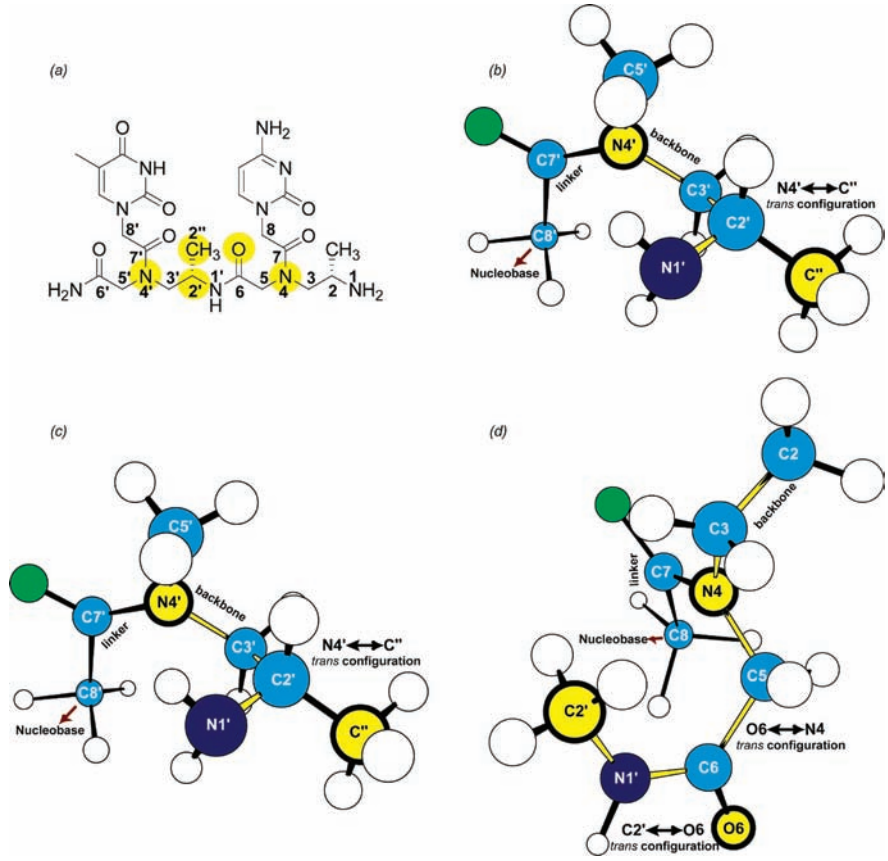

Figure 8. (a) Chemical structure of a CT γPNA dimer. (b−d) Energy minimized structures of the various subunits of this γPNA dimer, using the molecular mechanics force field MMX in HyperChem. Arrows indicate steric clashes between chemical groups forcing the backbone to adopt a right-handed helix. In addition to backbone steric constraints, the preferential configuration can be attributed to base-stacking coupled to geometrical restrictions centered at the chiral carbon, and these additively stabilize the helix. The nucleobases are omitted in the energy minimized structures for clarity, with emphasis on the backbone.

PNAs are hybrids of peptides and nucleic acids, comprised of peptide-like backbone and nucleic acids' nucleobases, they are structurally closer to peptides than they are to nucleic acids because of their acyclic backbone, and ease and flexibility of synthesis. Like peptides, just about any chemical group can be installed in the backbone, in particular, at the γ-position, allowing further selective tuning of their physical properties. Yet unlike peptides, PNAs contain nucleobases, which allow them to interact with one another in a sequence-specific and predictable manner in accordance with the Watson−Crick base-pairing rules. Molecules with such capabilities are valuable for biological and biomedical research and development, and for molecular engineering.[66−69] Perhaps the greatest asset of γPNAs is their ability to recognize double-stranded DNA through strand invasion, with the recognition occurring via Watson−Crick base-pairing.[37,38,51] The generality and specificity of their recognition along with the ease and flexibility of synthesis make γPNAs an attractive class of antigene reagents, as molecular tools for basic research as well as therapeutic and diagnostic reagents for the treatment and detection of genetic diseases.

Conclusion

The present results provide insights into how the structure of γPNA−DNA hybrid duplex influences the hybridization process, with emphasis on the introduced chiral γ-backbone modification. Installation of the chiral center at the γ-position forces the PNA backbone to adopt either a right-handed or a left-handed helix, depending on the stereochemistry as a result of steric clash between substituent at the C-2′ position and N4′. The helix is stabilized by sequential base-stacking, reinforced by the water spines that specifically bridge amide backbone with the adjacent N-terminus nucleobase. The chirality in the backbone is not competing with the preferred P-helical motif of PNA. These results agree with both the "constrained flexibility" concept for PNA, the suggestion that DNA is more flexible and adopts the PNA exigencies, and the high adaptability of the PNA backbone, in that it can accommodate chiral centers and a variety of chemical functionalities. Our structure provides a first glimpse into how single-stranded γPNAs are organized into helical motifs, and how helical sense is determined and propagated in a unidirectional fashion from C- to N-terminus. Such insights augment our chemical and structural knowledge to enhance the rational design of molecular "foldamers", with precise helical conformations and chemical functionalities

(66) Gartner, Z. J.; Tse, B. N.; Grubina, R.; Doyon, J. B.; Snyder, T. M.; Liu, D. R. *Science* **2004**, *305*, 1601–1605.
(67) Winssinger, N.; Ficarro, S.; Schultz, P. G.; Harris, J. L. *Proc. Natl. Acad. Sci. U.S.A.* **2002**, *99*, 11139–11144.
(68) Morrow, T. J.; Li, M.; Kim, J.; Mayer, T. S.; Keating, C. D. *Science* **2009**, *323*, 352.
(69) Opalinska, J. B.; Gerwirtz, A. M. *Nat. Rev. Drug Discovery* **2002**, *1*, 503–514.

needed to carry out specific biological functions, for binding as well as for catalysis.

Experimental Section

Synthesis. γPNA monomers were synthesized according to our established procedures starting with the appropriate Boc-protected L-amino acids.[31] PNA and γPNA oligomers were prepared on solid-support using standard Boc-chemistry.[70] The oligomers were purified by reverse-phase HPLC and characterized by MALDI-TOF mass spectrometry.

Crystallization. Prismatic crystals of γPNA−DNA duplex, 5 mg/mL in 50 mM Tris (pH 7.5), and 100 μM $ZnSO_4$ were grown in a reservoir solution that contained 20% (w/v) PEG-8000, 0.1 M Tris pH 8.5, and 0.2 M $MgCl_2$ using the vapor-diffusion method, in which 1 μL of duplex solution was added to 1 μL of reservoir solution in a hanging drop suspended over 0.7 mL of reservoir. To obtain metal-derivatized crystals for anomalous phasing, γPNA−DNA crystals were soaked with 5 mM $ZnSO_4$ in 25% (w/v) PEG-8000 with 0.1 M Tris pH 8.5 and 0.2 M $MgCl_2$ for 1 day. The soaked crystals were transferred to a cryo solution that contained 25% (w/v) PEG-8000, 0.1 M Tris pH 8.5, 0.2 M $MgCl_2$, and 20% ethylene glycol, and immediately flash-cooled in liquid nitrogen prior to data collection.

Data Collection, Structural Determination, and Refinement. A three-wavelength multiple-wavelength anomalous diffraction (MAD) data set was collected at the SER-CAT beamline ID-22 (Advanced Photon Source, Argonne National Laboratory, Table 1). At each wavelength, 180 images with 1° frame width were collected at a crystal-to-detector distance of 125 mm, and 5 s exposure times. The crystal was translated after each wavelength during data collection due to radiation sensitivity. All data sets were processed using HKL2000 suite and SCALEPACK;[71] data collection and processing statistics are reported in Table 1. Heavy atom positions were determined in the three-wavelength MAD data set and phased in SOLVE.[72] An unbiased $F_{obs}\, e^{i\varphi_{calc}}$ map obtained using the MAD phases showed continuous density for most of the backbone, permitting tracing of the duplex. Iterative cycles of restrained refinement in Refmac5[73] were followed by model fitting into $2F_{obs} - F_{calc}$ and $F_{obs} - F_{calc}$ maps at each refinement stage. Model building and fitting were done in Coot, and additional solvent and substrate molecules were added using ARP/wARP programs, which are part of the CCP4 program suite.[74] The current model has been refined to an $R_{work/free}$ of 21.2/23.5%. The asymmetric unit contains two independent molecules of 20 residues each, 815 nonhydrogen atoms, 257 water molecules, 5 zinc, and 5 magnesium atoms from crystallization condition; refinement statistics are reported in Table 1.

Multidimensional and Multinuclear NMR. Two dimensional NMR experiments were performed on a Bruker Avance DMX-500 instrument operating at 500.13 MHz for ^1H and 125.76 MHz for C^{13} for all monomers and isoleucine substructures, using standard pulse programs from the Bruker software library. The samples were prepared by dissolving 5 mg of dried monomers or submonomers in deuterated DMSO, otherwise stated. Each sample was then analyzed using 1D ^1H NMR, phase-sensitive double quantum filtered COSY (DQFCOSYPH), rotating frame Overhauser spectroscopy (ROESY), and ^1H,^{13}C heteronuclear single-quantum correlation spectroscopy (HSQC).

Acknowledgment. Financial support for this work was provided by the National Institutes of Health (GM076251) to D.H.L. and GM066466 to J.I.Y. and funded, in part, under a grant with the Pennsylvania Department of Health. We thank Dr. Ehmke Pohl of Durham University for his assistance with structural analysis and the staff members at the General Medicine and Cancer Institutes Collaborative Access Team (GM/CA-CAT) and the Southeast Regional Collaborative Access Team (SER-CAT), both at the Advanced Photon Source, Argonne National Laboratory for access and technical assistance. GM/CA CAT has been funded in whole or in part with Federal funds from the National Cancer Institute (Y1-CO-1020) and the National Institute of General Medical Science (Y1-GM-1104). Use of the Advanced Photon Source is supported by the U.S. Department of Energy, Office of Science, Office of Basic Energy Sciences, under Contract No. W-31-109-Eng-38. The NMR instrumentation at Carnegie Mellon University was partially supported by NSF (CHE-013093). Teragrid resources were provided by the Pittsburgh Supercomputing Center (TGMCB070070N).

Supporting Information Available: Additional figures and tables. This material is available free of charge via the Internet at http://pubs.acs.org.

JA907225D

(70) Christensen, L.; Fitzpatrick, R.; Gildea, B.; Petersen, K. H.; Hansen, H. F.; Koch, T.; Egholm, M.; Buchardt, O.; Nielsen, P. E.; Coull, J.; Berg, R. H. *J. Pept. Sci.* **1995**, *1*, 175–183.
(71) Otwinowski, Z.; Minor, W. *Methods Enzymol.* **1997**, *276*, 307–327.
(72) Terwilliger, T. C.; Berendzen, J. *Acta Crystallogr., Sect. D* **1999**, *55*, 849–861.
(73) Murshudov, G. N.; Vagin, A. A.; Dodson, E. J. *Acta Crystallogr., Sect. D* **1997**, *53*, 240–255.
(74) Perrakis, A.; Sixma, T. K.; Wilson, K. S.; Lamzin, V. S. *Acta Crystallogr., Sect. D* **1997**, *53*, 448–455.